DUDLEY KNOX LIBRARY
NAVAL POSTGRADUATE SCHOOL
MONTEREY CA 93943-5101

DUDLEY KNOX LIBRARY
NAVAL POSTGRADUATE SCHOOL
MONTEREY CA 93943-5101

Approved for public release; distribution is unlimited

Underwater Sound Radiation From Single Large Raindrops at Terminal Velocity; The Effects of a Sloped Water Surface at Impact

by

Glenn A. Miller

Lieutenant, United States Navy
B.S., United States Naval Academy, 1986

Submitted in partial fulfillment of the
requirements for the degree of

MASTER OF SCIENCE IN ENGINEERING ACOUSTICS

from the

NAVAL POSTGRADUATE SCHOOL

December, 1992

Anthony A. Atchley, Chairman,
Engineering Acoustics Academic Committee

Unclassified

Security Classification of this page

REPORT DOCUMENTATION PAGE

1a Report Security Classification Unclassified		1b Restrictive Markings	
2a Security Classification Authority		3 Distribution Availability of Report: Approved for public release; distribution is unlimited.	
2b Declassification/Downgrading Schedule			
4 Performing Organization Report Number(s)		5 Monitoring Organization Report Number(s)	
6a Name of Performing Organization Naval Postgraduate School	6b Office Symbol *(If Applicable)* 33	7a Name of Monitoring Organization Naval Postgraduate School	
6c Address *(city, state, and ZIP code)* Monterey, CA 93943-5000		7b Address *(city, state, and ZIP code)* Monterey, CA 93943-5000	
8a Name of Funding/Sponsoring Organization NPS	8b Office Symbol *(If Applicable)*	9 Procurement Instrument Identification Number	
8c Address *(city, state, and ZIP code)*		10 Source of Funding Numbers	
		Program Element Number / Project No / Task No / Work Unit Accession No	

11 Title *(Include Security Classification)* UNDERWATER SOUND RADIATION FROM SINGLE LARGE RAINDROPS AT TERMINAL VELOCITY; THE EFFECTS OF A SLOPED WATER SURFACE AT IMPACT.

12 Personal Author(s) Glenn A. Miller

13a Type of Report	13b Time Covered	14 Date of Report *(year, month,day)*	15 Page Count
Master's Thesis	From To	December 1992	51

16 Supplementary Notation The views expressed in this thesis are those of the author and do not reflect the official policy or position of the Department of Defense or the U.S. Government.

17 Cosati Codes			18 Subject Terms *(continue on reverse if necessary and identify by block number)*
Field	Group	Subgroup	spectral energy density, primary bubbles, Type I and Type II mechanisms, aerosol time gap

19 Abstract *(continue on reverse if necessary and identify by block number*

Previous studies have shown that terminal velocity raindrops striking a smooth water surface create oscillating bubbles that radiate significant underwater sound energy. Those studies identified two diameter ranges that produce bubbles: small drops (.8-1.1 mm diameter) which produce bubbles by one mechanism and large drops (2.2-4.6 mm diameter) which create bubbles by a different mechanism. Effects of oblique incidence have been studied only for small drops. Average energy spectra were calculated for a range of raindrop sizes striking a smooth water surface.

This work deals with the real life situation of large raindrops of a size often present in heavy rainfall (4.6 mm diameter) striking a sloped water surface. Terminal velocity is used to simulate natural rainfall, and the sloped surface is used to simulate the surface gravity waves of a natural sea. The effects of a sloped water surface on frequency spectra and energy for 4.6 mm raindrops are estimated.

By comparing energy spectra generated by single drops in an anechoic laboratory tank to underwater sound spectra measured at sea, it will be possible to estimate heavy rainfall rate by means of remote underwater listening devices.

20 Distribution/Availability of Abstract	21 Abstract Security Classification	
[X] unclassified/unlimited [ ] same as report [ ] DTIC users	Unclassified	
22a Name of Responsible Individual Herman Medwin	22b Telephone *(Include Area code)* (408) 624-1775	22c Office Symbol PH/Md

DD FORM 1473, 84 MAR 83 APR edition may be used until exhausted

All other editions are obsolete

security classification of this page Unclassified

ABSTRACT

Previous studies have shown that terminal velocity raindrops striking a smooth water surface create oscillating bubbles that radiate significant underwater sound energy. Those studies identified two diameter ranges that produce bubbles: small drops (0.8-1.1 mm diameter) which produce bubbles by one mechanism and large drops (2.2-4.6 mm diameter) which create bubbles by a different mechanism. Effects of oblique incidence have been studied only for small drops. Average energy spectra were calculated for a range of raindrop sizes striking a smooth water surface.

This work deals with the real life situation of large raindrops of a size often present in heavy rainfall (4.6 mm diameter) striking a sloped water surface. Terminal velocity is used to simulate natural rainfall, and the sloped surface is used to simulate the surface gravity waves of a natural sea. The effects of a sloped water surface on the frequency spectra and energy for 4.6 mm raindrops are estimated.

By comparing energy spectra generated by single drops in an anechoic laboratory tank to underwater sound spectra measured at sea, it will be possible to estimate heavy rainfall rate by means of remote underwater listening devices.

TABLE OF CONTENTS

I. INTRODUCTION 1

II. LABORATORY FACILITIES 4

A. EXPERIMENTAL SETUP 4

1. Drop Shaft 4
2. Intravenous (IV) Dropper 5
3. Anti-Wind Tube 5
4. Anechoic Tank 5
5. Wave Generator Frame and Motor 6
6. Video Camera 6
7. Hydrophone 7
8. Amplifiers and Filters 7
9. ComputerScope© 7

III. BACKGROUND 8

A. BUBBLE FORMATION MECHANISMS 8

1. Type I 8
2. Type II 8

B. ENERGY EQUATIONS 11

1. Conversion of Hydrophone Voltage to Pressure 11
2. Corrections to Pressure Signal 11
   a. Correction to One meter on Axis 11
   b. Near Field Correction (NFC) 12
   c. Percentage Correction Factor 12
   d. Summary 13
3. Spectral Analysis and Total Energy 13
4. Energy Calculation using the Theoretical Damping Constant and Peak Pressure 14

DUDLEY KNOX LIBRARY
NAVAL POSTGRADUATE SCHOOL
MONTEREY CA 93943-5101

IV. RESULTS 16
A. Energy using the Theoretical Damping Constant and Peak Pressure 17
1. Energy at Higher Frequencies 17
2. Time Gap 17
B. SPECTRAL ANALYSIS 22
1. Smooth vs Roughened Surfaces 22
2. Roughened Surface Categorized by Slope 24
V. CONCLUSIONS 26
VI. RECOMMENDATIONS 27
A. DEFINITIONS 27
1. Primary 27
2. Type I Mechanism 27
3. Type II Mechanism 27
B. FUTURE EXPERIMENTS 27
1. More Data for this Experiment 27
2. Multiple Raindrops 27
3. Multiple Hydrophones 28
4. Capillary waves 28
5. Eliminate the % Correction Factor 28
APPENDIX A 29
REFERENCES 41
INITIAL DISTRIBUTION LIST 43

ACKNOWLEDGMENTS

I would like to express my gratitude to my family, Tracy, G.A., and Savannah, for understanding why I disappeared for hours at a time during the last few weeks of the quarter. A special thanks goes to Tracy for buying the computer.

A few additional people helped make this thesis possible. My advisor, Dr. Herman Medwin, and co-advisor, Dr. Jeffrey Nystuen, offered valuable direction and advice. I also thank Prof. Medwin for funding my trip to New Orleans to present this paper to the Acoustical Society of America. An extra thanks goes to Jeff for accomplishing in thirty minutes what the EE department could not accomplish in three quarters; he made signal processing understandable (somewhat).

Collection of the roughened surface data would not have been possible without the assistance of Jeff and Mike Cook. George Jaksha always proves to be an invaluable source for anything mechanical or slightly creative.

I would like to thank Mr. Tarry Rago for analyzing salinity samples and the Monterey Bay Aquarium for providing the sea water.

Finally, I would like to thank those individuals not directly affiliated with my work but willing to listen to me think out loud (and sometimes tell me to shut up), Dr. Robert Keolian, Lt. Rick Lawrence, USN, and Capt. Ron Stockermans, CAF.

I. INTRODUCTION

One of the goals of the Naval Postgraduate School (NPS) Raindrop Lab is to understand the physics of underwater sound production by natural rainfall. Previous studies have shown that significant underwater sound is generated by the impact of raindrops upon a water surface and even more so by oscillating bubbles, when formed [Franz, 1959]. Once the sound pressure is measured, the energy spectrum of a single drop can be calculated. Figure 1.1 shows a typical time signal of an impact of a large diameter (4.6 mm) drop which produced two bubbles . The corresponding energy spectrum is also shown.

By cataloging the sound produced by each raindrop size, it is possible to predict the sound produced by natural rainfall [Nystuen *et al* 1992]. This, in turn, will allow rainfall to be monitored using passive listening devices.

Raindrops can be categorized by size and acoustic signal [Medwin *et al*, 1992]. Table 1.1 summarizes the common drop size categories and their corresponding sources of sound.

TABLE 1.1. Raindrop Sizes and their Sources of Sound.

Nomenclature	Raindrop Diameter (mm)	Sources of Underwater Sound
Minuscule	0-0.8	Impact
Small (Type I)	0.8-1.1	Impact and Bubbles
Mid-Size	1.1-2.2	Impact
Large (Type II)	2.2 and larger	Impact and Bubbles

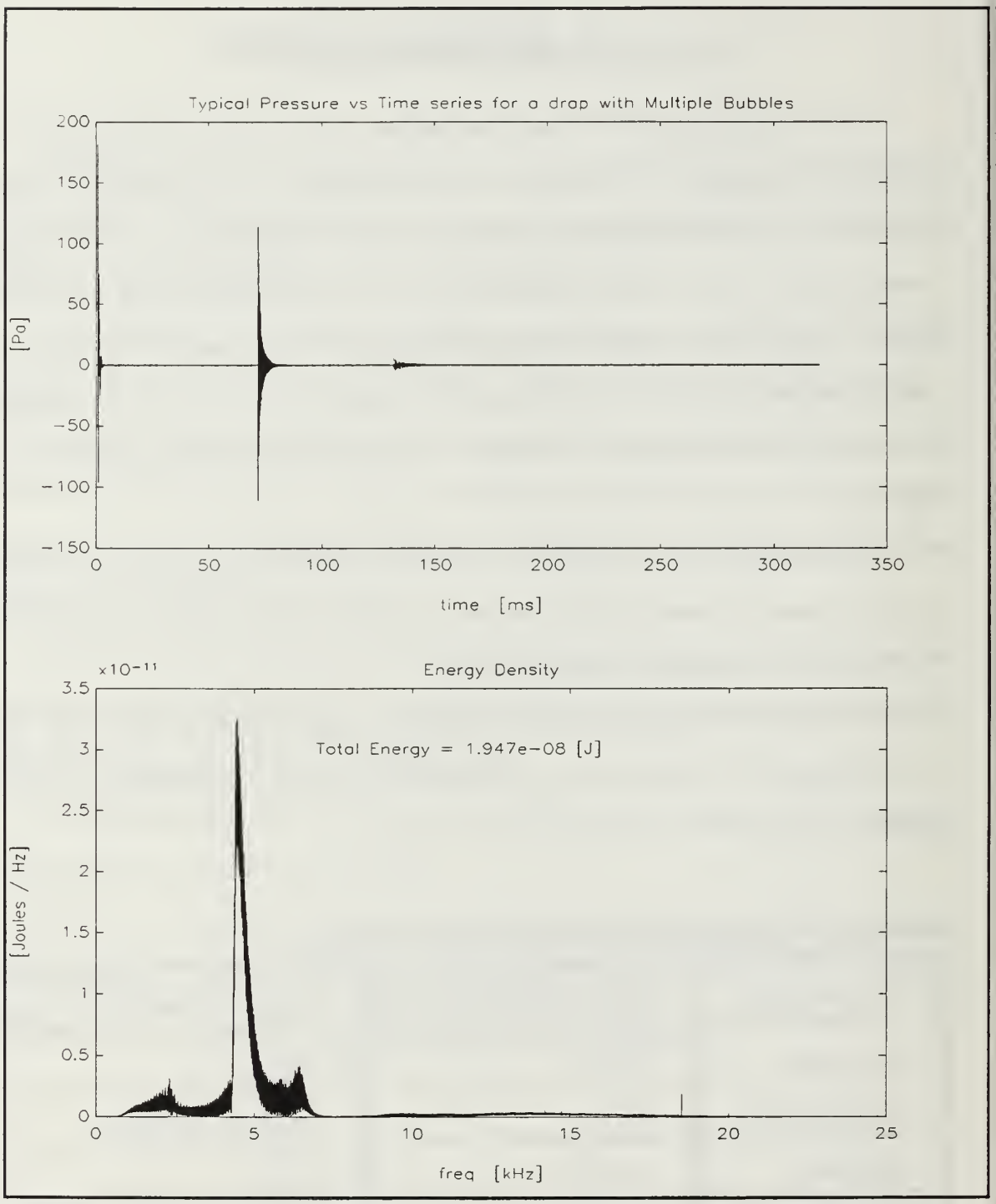

Figure 1.1. Typical graph of a time series of on-axis acoustic pressure at 1 m for an impact and two resulting bubbles (upper plot) and the corresponding energy spectrum (lower plot). {Sampling frequency 50 kHz.; 4.6 mm drop}.

The most important size categories are small and large drops as these two sizes consistently produce oscillating bubbles which are the dominant sound source. (The Type I and Type II bubble formation mechanisms are described in Chapter III.)

All experiments at NPS have been conducted with raindrops at terminal velocity. Previously, however; the large drops were impacting at normal incidence upon smooth water surfaces. A normal angle of incidence does not describe a natural sea state. Although these experiments were outstanding for determining the basic physics of underwater sound production, a more realistic scenario is required.

Kurgan [1989] conducted experiments for small drops at terminal velocity and at various angles of incidence. The influence of angle of incidence on small drops was very significant. His non-normal incidence angles were generated by placing a fan above the point of impact and forcing the small drops to strike the smooth surface at an oblique angle. Logistically large raindrops can not be significantly deflected using a fan.

The purpose of this thesis is to apply the theory and knowledge gained from past experiments with smooth surfaces to large raindrops impacting upon a sloped water surface. This simulates ocean surface gravity waves. Large drops, with a diameter of 4.6 mm at terminal velocity, were used throughout the experiment. The results will be compared to those for smooth surface experiments.

II. LABORATORY FACILITIES

A. EXPERIMENTAL SETUP

1. Drop Shaft

The laboratory facilities available for this experiment are unique to the Naval Postgraduate School. A utility shaft with a height of 26 meters (and cross section of 3 m x 3 m) empties into a room containing a 1.5 m diameter, redwood lined anechoic cylindrical tank . [Figure 2.1] Installed in the shaft is a 9" diameter plastic tube that reduces the amount of interference from air drafts. The 26 m height allows drops of all sizes normally found in natural rainfall to reach terminal velocity.

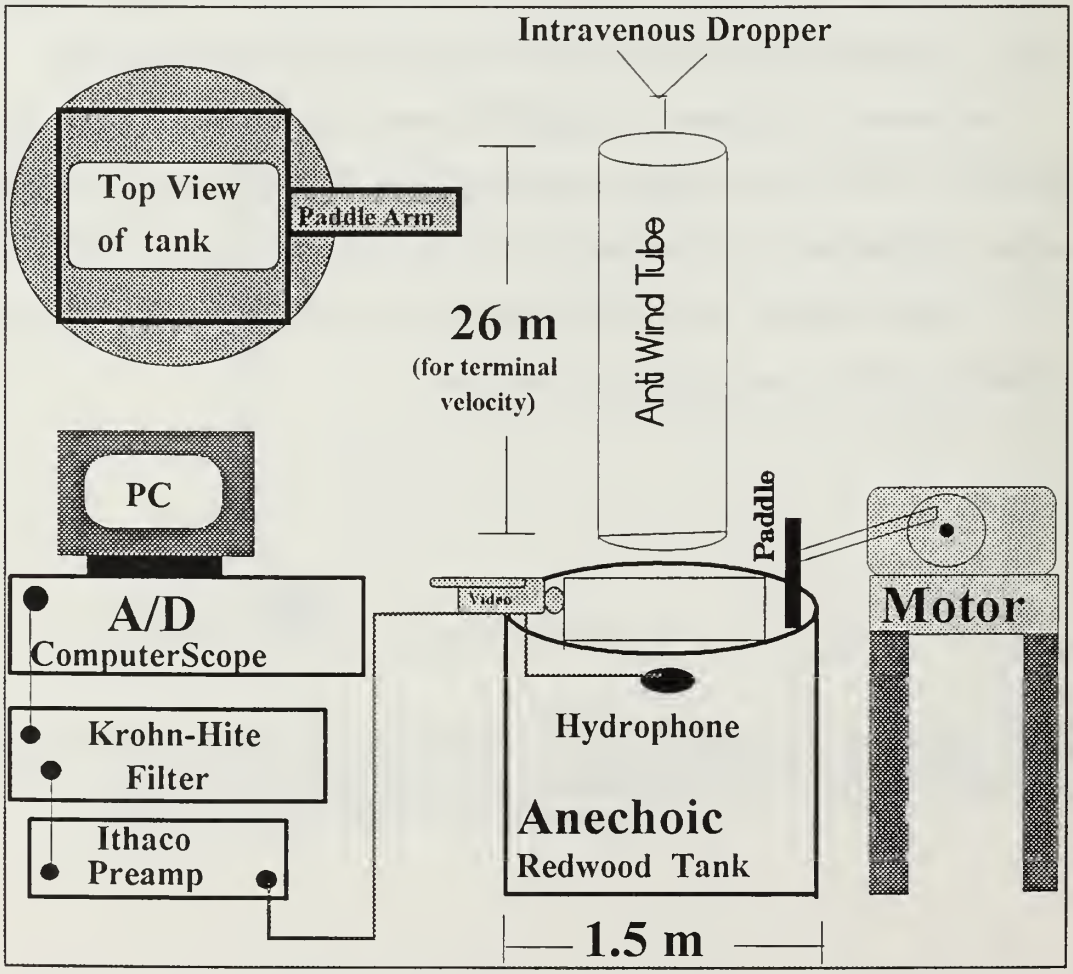

Figure 2.1. Diagram of Laboratory Setup.

2. Intravenous (IV) Dropper

A standard medical IV bag with surgical tubing is used to generate large raindrops. Attached to the tubing is a tip calibrated to produce 50 μL drops (4.6 mm diameter). The accuracy of the tip was verified by measuring the volume of 100 drops six times. Each repetition was ± 5 % of the volume expected for 100 drops.

3. Anti-Wind Tube

New to the lab is the anti-wind tube. It is constructed of thirty-three needlepoint hoops (nine inch diameter) and two 50 ft. lengths of typical plastic liner for gardens. The two lengths are overlapped by 13 feet. The hoops are equally spaced the entire length of the tube. The inner ring of the hoop is rolled inside of the plastic. The outer ring is made tight around the inner ring. This forms the plastic into a 9" x 87' cylinder.

The addition of the tube increases the accuracy of the impact of the raindrop in relation to the location of the hydrophone. Previous work measured impacts with estimates of the random horizontal distances from the hydrophone (within 20 cm). Presently, we are consistently able to impact the surface of the water within 4 cm of the epicenter of the underwater hydrophone. The increased accuracy reduces the amount of range and angle correction required.

4. Anechoic Tank

In the room where the anti-wind tube ends is a cylindrical redwood tank with a diameter and a height of 1.5 m. The tank is made anechoic with a lining of redwood wedges. The tank contains filtered salt water acquired from the Monterey Bay Aquarium. Because data sets were taken on different days, the salinity was measured for each data set.

The tank houses the wave generator frame and an LC-10 hydrophone.

5. Wave Generator Frame and Motor

Also new to the lab is the wave generator frame and motor. It is inserted into the tank and resembles a box kite. It is constructed of a redwood frame that supports walls made of Mylar. Three sides are stationary while the fourth Mylar wall is hinged at the bottom to allow for a paddle motion. The paddle is attached to a motor mounted level with the top of the tank. The dimensions of the frame are 26" x 26" x 41" (L x W x H).

The wave generator remains in the tank for experiments involving both smooth and rough surfaces. Mylar was used because of its anechoic properties. It allows sound to pass but reflects surface water waves. This maintains the anechoic integrity of the tank and still allows for the creation of a roughened surface.

The motor's shaft generates circular motion. This motion is translated to "linear" motion to drive the paddle via a mechanical eccentric coupling.

6. Video Camera

A Sony 8 mm video camera placed level with the water surface is used to film the sloped surface experiment. Extracted from the videotape are the slope of the surface and the depth of the hydrophone at the time of impact. The camera speed is 30 frames per second.

To assist with the determination of the slope, a grid of vertical strings is suspended in the tank . The grid is filmed in the background while the drops impact the surface. The spacing between vertical lines is 2 cm. A reference line is marked on the grid before the surface is roughened. This allows for the measurement of the depth of the hydrophone.

7. Hydrophone

An LC-10 hydrophone [Figure 2.2] from Celesco Transducer Products, Inc. is used to measure the sound pressure of the impacts and oscillating bubbles. It is positioned at a depth of 6 cm for both types of experiments. For the sloped surface experiment a video camera is used to determine the instantaneous depth of the LC-10. The hydrophone is suspended by three supports of fishing line. The supports are positioned at intervals of 120° to minimize the amount of movement caused by a passing wave.

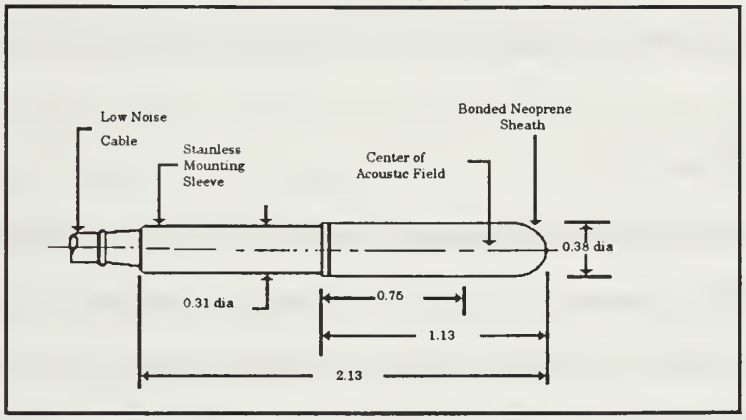

Figure 2.2. LC-10 Hydrophone (All dimensions are in inches).

8. Amplifiers and Filters

The signal from the hydrophone is connected to an Ithaco 1201 Pre-amp set at a gain of 100. The signal is then connected to a Krohn-Hite 3202R band pass filter. The frequencies passed are between 1 kHz and 30 kHz in both pieces of equipment.

9. ComputerScope©

The signal is then connected to an IBM clone 286 computer with an analog to digital converter (A/D). The digital data acquisition card and its software, ComputerScope (sold by RC Electronics), is used for all data acquisition.

Amplitude resolution was twelve bits. The sampling frequency used was 50 kHz. This allowed for a time series of 320 ms duration. Previous work was sampled at 125 kHz and 250 kHz. Their respective time series lengths were 128 ms and 64 ms.

III. BACKGROUND

A. BUBBLE FORMATION MECHANISMS

Two distinct bubble formation mechanisms have been identified [Snyder, 1990]. The Type I mechanism pertains to small diameter raindrops (0.8 mm to 1.1 mm) whereas the Type II mechanism pertains to large diameter raindrops (> 2.2 mm). At terminal velocity the raindrop diameter ranges of $d < 1.1$ mm and $1.1 \text{ mm} < d < 2.2$ mm do not produce bubbles.

1. Type I

Small raindrops at terminal velocity produce Type I bubbles 100 % of the time when striking a smooth surface at a normal angle of incidence. As the angle of incidence increases to 20°, the bubble formation percentage drops to 10 % [Kurgan, 1989]. A Type I bubble is formed when the base of a conical splash crater is pinched off [Longuet-Higgins, 1990]. The resulting bubble resonates at approximately 15 kHz. Additional references for the Type I mechanism are Pumphrey *et al.*, [1989] and Oguz and Prosperetti, [1990]. This mechanism can be used to explain the sound produced underwater by light rain [Pumphrey *et al*, 1989] and the influence of wind upon the sound produced underwater by light rain [Nystuen, 1977].

2. Type II

The Type II mechanism is important when large raindrops are present in the rain. Large raindrops are prevalent during heavy rain.

Type II bubbles are not formed as consistently as Type I bubbles. At terminal velocity and normal incidence upon a smooth water surface, it has been shown that 4.6 mm drops form at least one bubble 50-65 % of the time. When Type II bubbles are

formed they resonate between 1.6 and 10 kHz [Jacobus,1991; Ostwald, 1992] depending on drop diameter. For 4.6 mm drops, the dominant resonance frequencies are between 1.6 and 2.0 kHz.

Snyder, Jacobus, and Ostwald describe Type II bubbles. They define a primary bubble as the bubble that produces the largest peak to peak voltage (pressure) for that drop when produced by the Type II mechanism (usually 60-70 ms after impact). Secondary bubbles were defined as anything else. We have found that this may not be appropriate. It would be better to define the "primary bubble" as the resulting bubble that contains the most energy. This definition is independent of the bubble production mechanism. Recent experiments with large drops have shown that some previously defined "primary" bubbles may have been produced by the Type I mechanism generated by late-arriving aerosols resulting from the impact. The long time after impact (>100 ms) when a newly defined primary bubble begins to resonate leads us to believe that it is most likely generated by a Type I mechanism (generated by a small drop, an aerosol, striking the surface). Chapter IV addresses the significant effect of a sloped surface on these "late" bubbles.

Figure 3.1 (frames 1-10) shows the sequence of events that lead to the formation of a Type II bubble. This phenomenon was first observed by Snyder [1990]. Slow motion and stop motion photography of 400 frames per second allowed Snyder the opportunity to sketch the sequence .

Frames 1 and 2: A flattened raindrop at terminal velocity impacts a smooth water surface and begins to form a canopy. The splash generates numerous aerosols.

Frames 3 and 4: The canopy continues to form above the splash crater.

Frames 5, 6, and 7: Water continues to flow up the sides of the canopy and the convergence of water forms upward and downward moving turbulent jets.

Frames 8 and 9: The downward moving jet plunges through the bottom of the crater.

Frame 10: This jet contains entrained air. A buoyant force causes the entrained air to break off and form a resonating bubble. This action occurs only if the downward moving jet is canted.

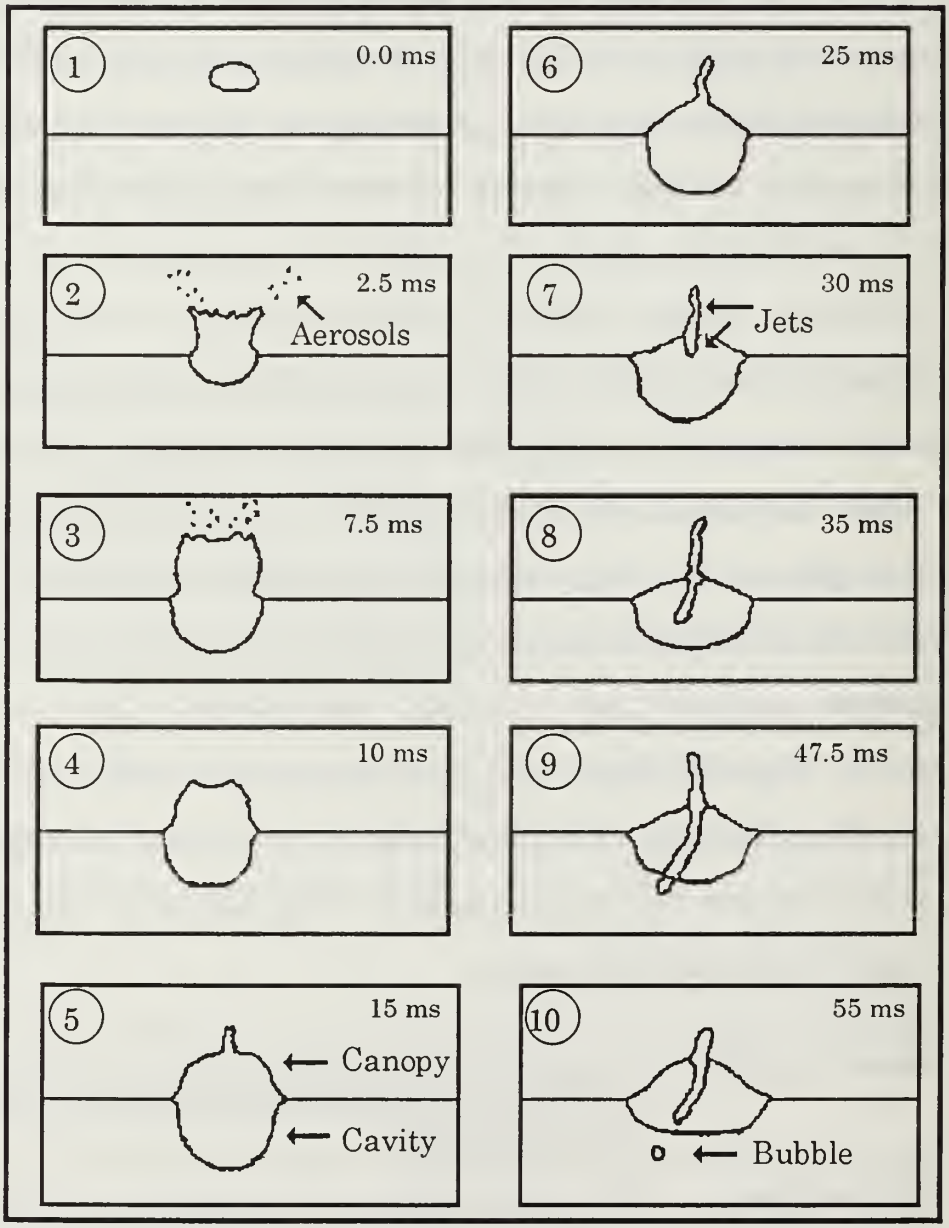

Figure 3.1. Bubble Formation by the Type II Mechanism.

B. ENERGY EQUATIONS

1. Conversion of Hydrophone Voltage to Pressure

To calculate energy, the hydrophone voltage signal must first be converted to a pressure signal. This is done using Equation 3.1,

$$p_{hyd} = \frac{v}{G \bullet ML} \qquad (3.1)$$

where p_{hyd} is the pressure at the hydrophone [Pa], v is the hydrophone voltage [volts], G is the amplifier gain, and ML is the hydrophone sensitivity level [volts/Pa].

2. Corrections to Pressure Signal

a. Correction to One meter on Axis

i. Dipole Radiation Pattern. Kurgan [1989] showed that the bubble oscillation pattern was that of a dipole (cos θ term). The geometry of the problem is shown in Figure 3.2.

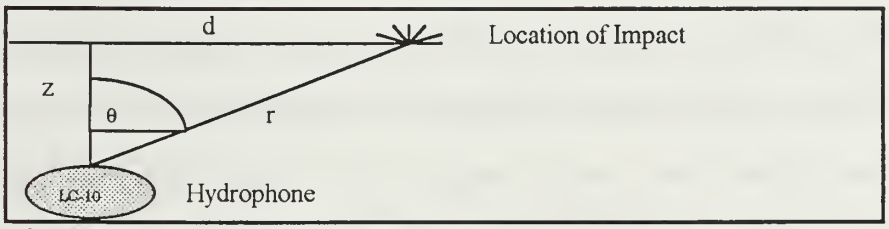

Figure 3.2. Location of Impact with respect to the Hydrophone.

ii. Spherical Spreading. A correction is applied to account for the 1/r divergence.

Therefore, all pressures measured at range **r** and depth **z** were converted to 1 meter on axis using Equation 3.2 where r_0 = 1 m and cos θ = z/r.

$$p_{1m\ axis} = \frac{p_{hyd}}{\cos\theta} \frac{r}{r_0} \qquad (3.2)$$

b. Near Field Correction (NFC)

Because the hydrophone was within a fraction of a wavelength, an error between the measured pressure field and the pressure corrected to 1 meter on axis can occur. This can be corrected in the frequency domain using Equation 3.3 [Medwin and Beaky, 1989],

$$NFC = \sqrt{\frac{1}{1+\frac{1}{(kr)^2}}} \tag{3.3}$$

where k is the wave number ($2\pi/\lambda$ [m^{-1}]) and r is the range [m] as shown in Figure 3.2.

c. Percentage Correction Factor

The voltage time series of a single drop was recorded if it produced at least one bubble. Then the energy was calculated and averaged for all drops in the data set. However, because only data from drops producing bubbles were taken and the fact that raindrops do not produce Type II bubbles 100 % of the time, the average spectral density was obtained by multiplying the calculated energy spectrum by a percentage correction factor equal to the percentage of drops which produced bubbles (determined separately). Jacobus and Ostwald extracted the impact and resonating bubbles from each time series. They then calculated the average energies due to impacts only, and then repeated the process for bubbles only. Jacobus showed that the impact energies are significantly less than bubble energies (approximately four orders of magnitude). To obtain the "average" spectral energy due to bubbles, the percentage correction factor was applied to the calculated bubble spectrum.

This work does not separate the impacts and bubbles from the time series and applies the percentage correction factor to the energies calculated from the entire series. The error in this approach is considered insignificant.

d. Summary

Equation 3.4 shows all correction factors (except the percentage correction factor) considered at the same time for the pressure series.

$$P_{1\ m\ on\ axis\ farfield} = \frac{r}{G\ ML\ r_o\ \cos\theta}\ NFC\ \left|V(f)\right| \qquad (3.4)$$

V(f) is the Fourier transform of the voltage-time series. Equation 3.4 combines equations 3.1, 3.2, and 3.3. The percentage correction factor is later applied to the ensemble energy density, rather than to each individual drop saved as data.

3. Spectral Analysis and Total Energy

A quantity proportional to the energy density spectrum can be calculated using Equation 3.5 [Ostwald, 1992].

$$E(f) = \frac{2\ \Delta t}{N\ df}\ \left|P_{1\ m\ on\ axis\ farfield}(f)\right|^2 \qquad \left[\frac{\mathrm{Pa}^2\ s}{Hz}\right]\ ,\ f \geq 0 \qquad (3.5)$$

N is the number of points in the FFT and the frequency resolution is given by df=1/(N Δt).

To convert the units to Joules/Hz, Equation 3.6 was used [Ostwald, 1992]. This is the energy spectral level as a function of frequency, and a subscript is added to avoid confusion with Equation 3.5.

$$E_f = \frac{2\pi r^2}{3\ \rho_o c}\ E(f) \qquad \left[\frac{\mathrm{J}}{\mathrm{Hz}}\right] \qquad (3.6)$$

This is the evaluation of the energy density as shown in the bottom half of Figure 1.1.

The total energy is calculated using Equation 3.7. The subscript "s" is used to designate a spectral calculation and to avoid confusion with the energy (E_δ) which is calculated in the next section by using the measured theoretical damping constant (δ) and the peak pressure in the time domain.

$$E_s = \frac{2\pi\ r^2}{3\ \rho_0 c} \sum_{f=0}^{f_{max}} E_f\ df \qquad [J] \tag{3.7}$$

4. Energy Calculation using the Theoretical Damping Constant and Peak Pressure

A combination of equations derived by Kurgan [1989] and Scofield [1992] offers another method to calculate the energy of an individual bubble at a given frequency from the peak axial pressure and the damping constant. The combination is derived assuming dipole radiation and the theoretical damping constant for a given bubble size. Previously, Kurgan empirically calcualted the energy and did not consider the damping constant. Scofield was interested only in the damping constant and did not consider the dipole nature of a bubble. From Figure 6.3.1 of Clay and Medwin [1977], one can show that for the frequencies of interest for this work, the damping constant (δ) can be approximated by $\delta = .0025\ f^{(1/3)}$ where the frequency is in Hz. The energy density on axis from an acoustic dipole [Scofield,1992] can be written as

$$E_d = \frac{p^2_{1\ m\ on\ axis}}{4\pi\rho_0 c f_o\ \delta} \qquad \left[\frac{J}{m^2}\right] \tag{3.8}$$

where the pressure is the PEAK pressure of the bubble time series.

The energy can be estimated by integrating Equation 3.8 (using a dipole radiation pattern) [Kurgan, 1989].

$$E_\delta = \iint E_d \cos^2\theta \, dA \qquad (3.9)$$

The elemental area is $\mathbf{dA = (2\pi\, r \sin\theta)(r\, d\theta)}$. Evaluation of Equation 3.9 yields the energy equation using the measured theoretical damping constant and peak pressure:

$$E_\delta = \frac{p_{1\,m\ on\ axis}^2 \; r^2}{6\rho_o c f_o \; \delta} \quad [J] \qquad (3.10)$$

IV. RESULTS

Smooth surface data was taken as well as sloped (roughened) surface data. It was observed that a sloped surface has a slightly higher percentage of at least one bubble being produced (70-73 %) than a smooth surface (50-65 %) for 4.6 mm diameter drops. The roughened surface data was analyzed as one data set and then again as three separate data sets broken into slope categories. A data set consists of a number of independent drops, falling at terminal velocity, and striking either a smooth or a sloped surface. A drop time series was saved for analysis if it produced at least one bubble. Because our time series extended further than ever before (320 ms), many more bubbles occurring later in time were detected. Jacobus' work only extended to 64 ms and Ostwald's time series ended at 128 ms. The duration of the series was governed by the available computer memory and the sampling rate of the data acquisition software (ComputerScope©). The sampling rates for Jacobus and Ostwald, respectively, were 250 kHz and 125 kHz. This work uses a sampling rate of 50 kHz. This rate is fast enough to avoid ambiguity in the signals with frequencies of interest and allows for a longer time series. The following presentation of our data will clearly show what we call the effects of a sloped water surface on the underwater sound radiation caused by large raindrops. For this thesis only the largest drop size most likely to occur in a natural, heavy rainstorm was used (4.6 mm diameter).

All energies were calculated using MATLAB, a matrix manipulation program by The MathWorks, Inc. Appendix A contains the programs used to gather, process, and plot all data. The spectral analysis method uses Equation 3.7. The damping constant and peak pressure (temporal) method uses Equation 3.10.

A. ENERGY using the THEORETICAL DAMPING CONSTANT and PEAK PRESSURE

The energy contained in dominant (primary) bubbles, as defined in earlier work [Jacobus,1991; Ostwald, 1992], was calculated for the smooth and roughened surface data by using Equation 3.10. Previously, the energy of only the dominant bubble of each series was calculated because Equation 3.4 requires knowledge of the angle θ and a range **r** from the hydrophone. Constrained by the initial definition of "primary bubble", only the range of the initial Type II bubble is known. Multiple hydrophones will be needed to accurately measure the range to all bubbles created. However, the use of the damping constant and the peak pressure to evaluate the energy for each bubble allows for an estimate of the energy in the entire series.

1. Energy at Higher Frequencies

Figure 4.1 (top) shows the same general distribution as reported by Ostwald. Figure 4.1 (bottom) shows that for a sloped surface at the time of impact, there exists more energy at higher frequencies. Higher frequency bubbles are produced by smaller raindrops [Kurgan, 1989; Jacobus, 1991; Ostwald, 1992]. Because they are higher frequency, one would assume that they are formed by the Type I mechanism (or late aerosol impacts). There is no definitive proof that this is the case. The roughened surface could possibly produce Type II bubbles with frequencies higher than previously observed.

2. Time Gap

As previously stated, earlier work used a shorter time series. When the duration of the series is extended, a noticeable time gap was observed for the smooth surface data. This gap occurs between 110 and 140 ms as suggested in Figure 4.2 (top). This time gap is not present in the roughened surface data [Figure 4.2, bottom].

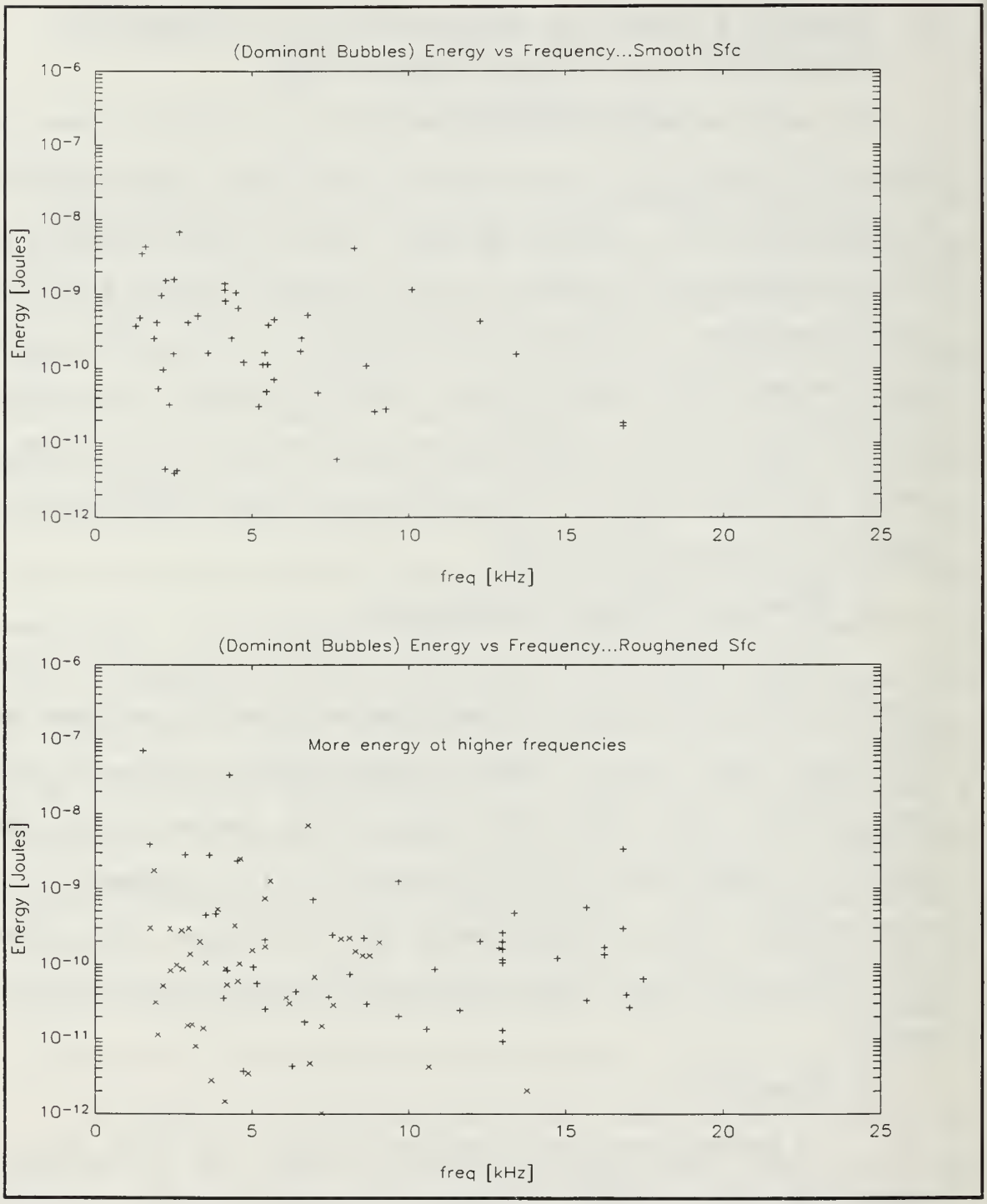

Figure 4.1. Comparison of Energies of Dominant Bubbles for Smooth (top) and Roughened (bottom) surfaces.

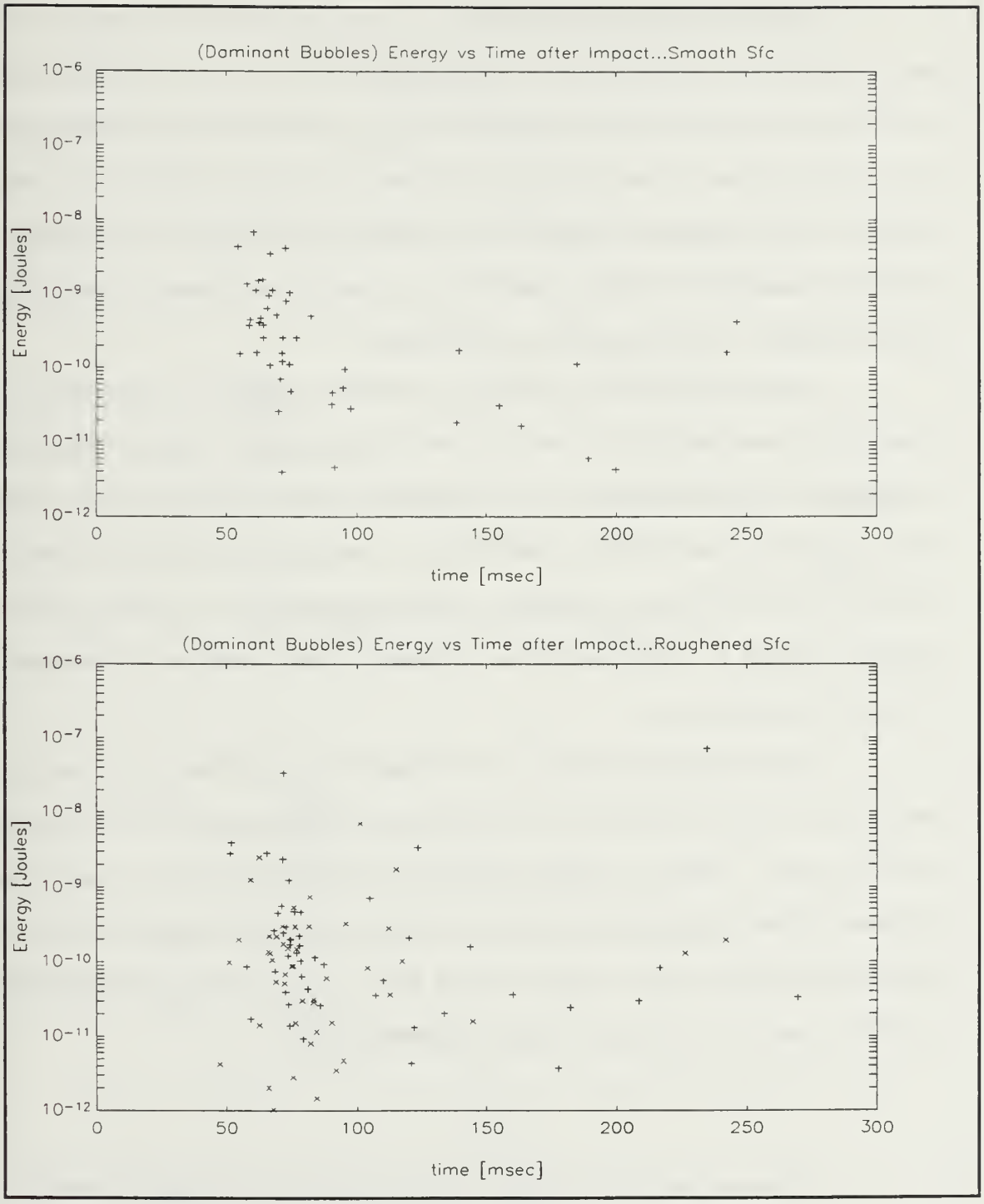

Figure 4.2. Comparison of Dominant Bubble Energy vs Time after Impact for Smooth (top) and Roughened (bottom) surfaces.

When the frequencies of all bubbles that were present in the time series (primary and secondary) are plotted against the time after impact, the time gap becomes more prevalent in the smooth surface data [Figure 4.3, top]. The end of the gap (approximately 140 ms after impact of the large drop) corresponds to the time delay for an aerosol trajectory with a maximum height of 2.5 cm. Bubbles occurring after 140 ms would not have been considered as dominant bubbles in previous studies. Because of the timing as shown in Figure 3.1, they can not be Type II bubbles.

Aerosols generated by impacting a smooth, stationary surface tend to be "launched" almost vertically and have been seen reaching extreme heights of 40 cm above the surface. This corresponds to a time of flight (time after impact) of 571 ms. Visually, the average height was between 12 and 15 cm. These heights correspond to times after impact of 312 and 350 ms, respectively. This suggests that the duration of the data collection should be lengthened further, although there would be a corresponding reduction in sampling rate.

For the roughened surface data in Figures 4.2 and 4.3 (bottom) the time gap is not present. This is consistent with a reduced time of flight caused by a lower trajectory of the aerosols. The rough surface aerosols are also launched with a much greater horizontal velocity component than the smooth surface aerosols. It was quite obvious that the horizontal velocity of the surface wave, as well as the wave slope, greatly affect the velocity components and the launch angles of these aerosols.

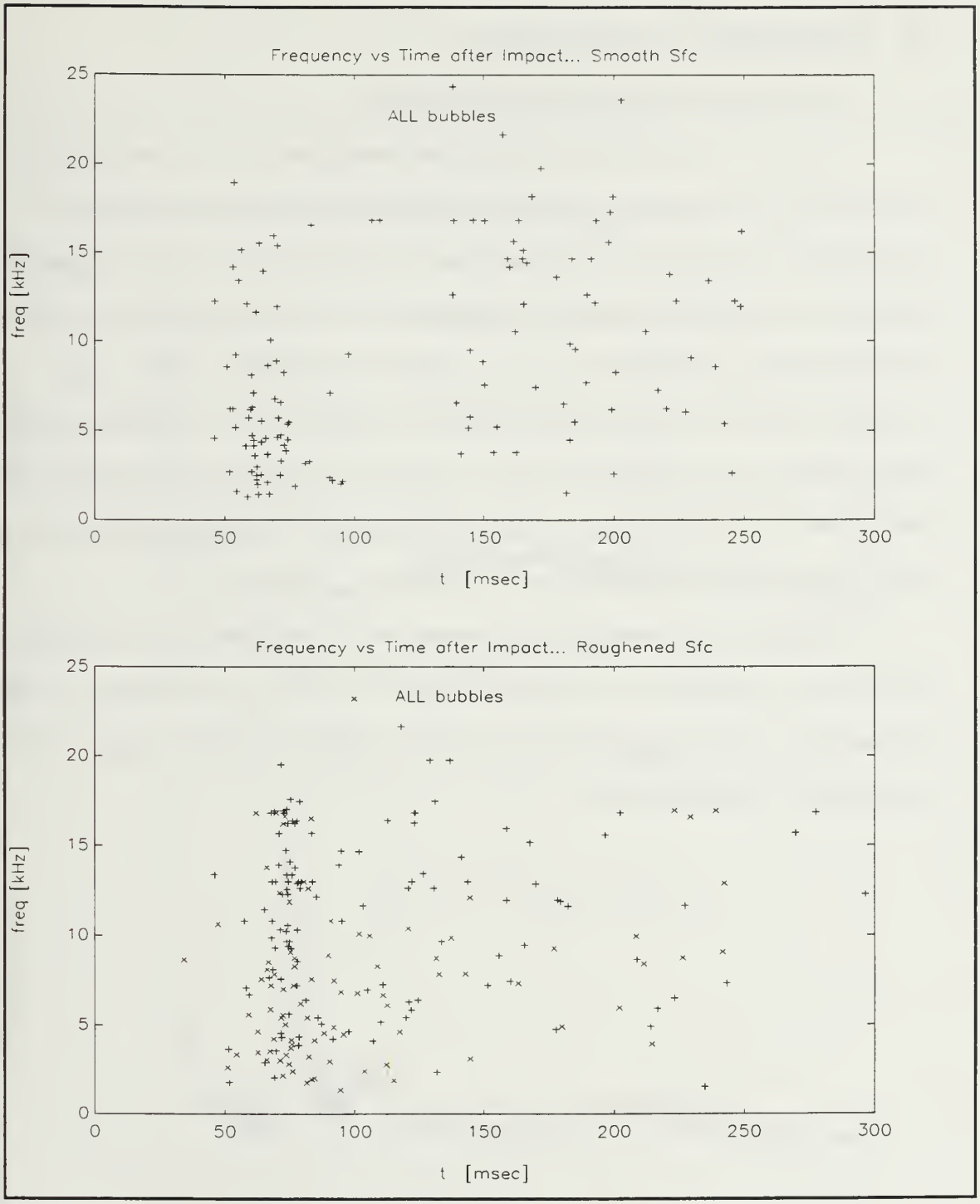

Figure 4.3 Comparison of Frequencies of ALL Bubbles vs Time after Impact for Smooth (top) and Rough (bottom) surfaces.

B. SPECTRAL ANALYSIS

1. Smooth vs Roughened Surfaces

Figure 4.4 compares the average spectral energy density of the smooth surface data (top half) to the average spectral energy density of the roughened surface data (bottom half). The instantaneous surface slope at the time of impact was not measured because we were looking for a general effect due to a randomly sloped surface. It can be seen from Figure 4.4 that the average total energies are comparable. This was not expected because more high frequency bubbles were observed in the roughened surface data compared to the smooth surface data. Typically, high frequency bubbles radiate less energy than low frequency bubbles; therefore their influence on the total energy is not as significant as lower frequency bubbles.

The plot of the average energy density for the roughened surface in Figure 4.4 (bottom) also demonstrates an apparent shift of the peak of the spectrum to higher frequencies. This was expected because of the presence of higher frequency bubbles occurring late in the time series.

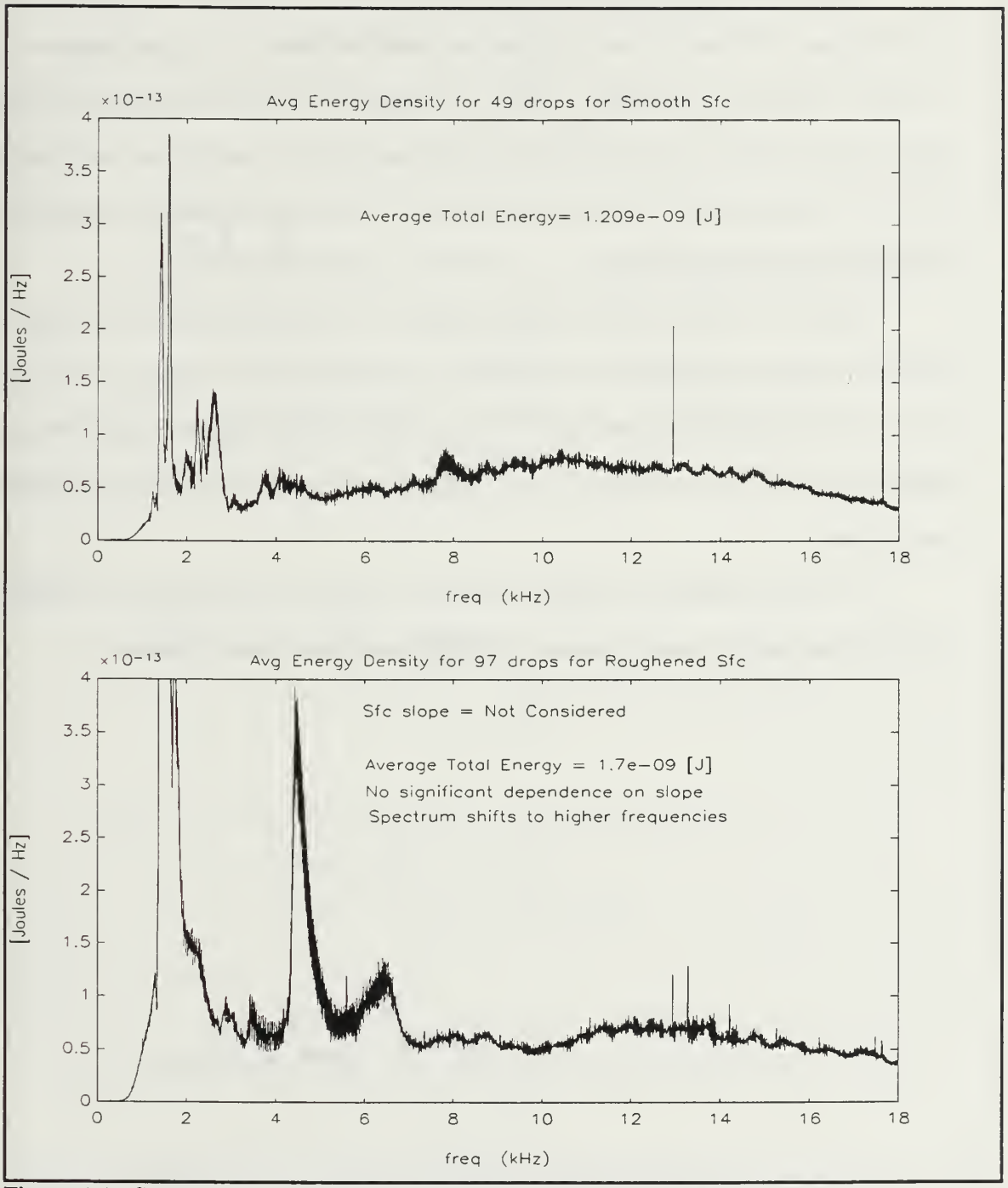
x10−13
Avg Energy Density for 49 drops for Smooth Sfc
Average Total Energy= 1.209e−09 [J]
[Joules / Hz]
freq (kHz)
x10−13
Avg Energy Density for 97 drops for Roughened Sfc
Sfc slope = Not Considered
Average Total Energy = 1.7e−09 [J]
No significant dependence on slope
Spectrum shifts to higher frequencies
[Joules / Hz]
freq (kHz)

Figure 4.4. Comparison of Average Energy Densities for Smooth (top) and Roughened (bottom) surfaces.

2. Roughened Surface Categorized by Slope

The use of a video camera allowed us to determine the slope of the surface at the time of impact. The slopes were grouped into three categories. The mean slopes were 0, 6, and 11° from the horizontal (± 3°). A 0° slope for a roughened surface is different from a smooth surface because of the horizontal velocity of the surface waves. The wave velocity was seen to be imparted to the raindrop at impact and affected the nature of the aerosols generated by the impact.

Figure 4.5 shows the three slope categories. It can be seen that the average total energies are again comparable, independent of the slope of the surface at the time of impact. Forty-eight drops were used for this analysis. The energies are all within one standard deviation of each other. Better statistics are needed before stronger statements can be made.

As with the randomly roughened surface of Figure 4.4, the peaks of the spectra of Figure 4.5 also shift to higher frequencies as the slope of the surface increases.

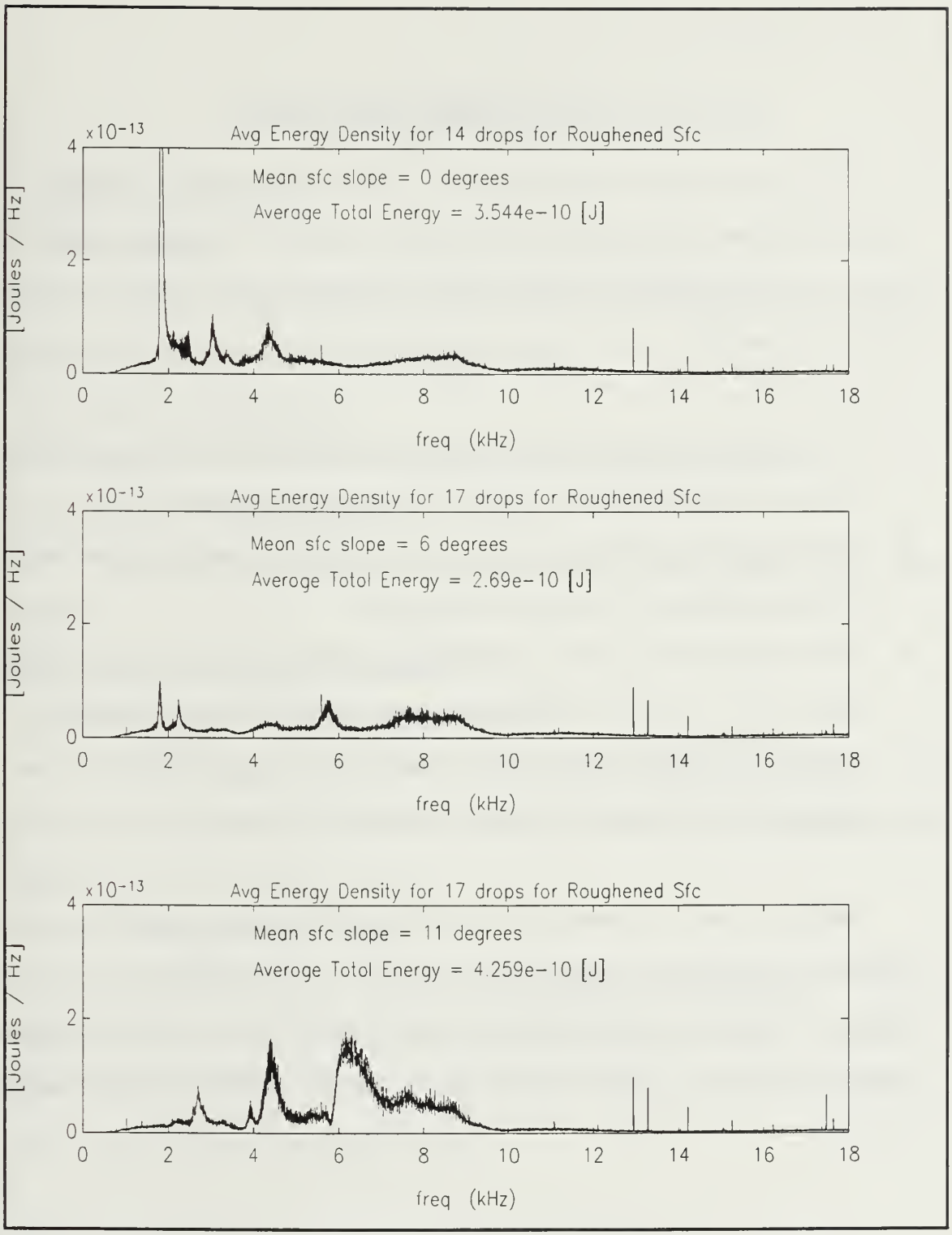
x10-13
Avg Energy Density for 14 drops for Roughened Sfc
Mean sfc slope = 0 degrees
Average Total Energy = 3.544e-10 [J]
[Joules / Hz]
freq (kHz)
x10-13
Avg Energy Density for 17 drops for Roughened Sfc
Mean sfc slope = 6 degrees
Average Total Energy = 2.69e-10 [J]
[Joules / Hz]
freq (kHz)
x10-13
Avg Energy Density for 17 drops for Roughened Sfc
Mean sfc slope = 11 degrees
Average Total Energy = 4.259e-10 [J]
[Joules / Hz]
freq (kHz)

Figure 4.5. Comparison of average energy densities of three surface slope categories.

V. CONCLUSIONS

The original purpose of this thesis was to determine the effects of a sloped water surface at the time of impact for a 4.6 mm diameter raindrop. While several effects were observed, this experiment also opens the door to numerous other studies. The results of this study reveal that:

- For smooth and rough surfaces (including slope categories): average energies per drop are of the same order of magnitude [Figure 4.4 and Figure 4.5].
- The peak of the energy spectrum for the sloped surface apparently shifts to higher frequencies [Figure 4.4, bottom and Figure 4.5].
- The "time gap" discovered for smooth surface data is absent for the sloped surface data. We now understand that the time gap is absent in the sloped surface data because the characteristics of sloped surface aerosols are greatly affected by the slope of the surface and the horizontal velocity of the surface wave.

Only after more is known about the physics of underwater sound produced by raindrops of different sizes generated in a laboratory, will we be able to understand the physics of underwater sound produced by natural rainfall at sea. This will ultimately establish the ability to estimate rainfall rate by means of remote underwater listening devices.

VI. RECOMMENDATIONS

A. DEFINITIONS

1. Primary

Redefine *Primary (dominant)* to be the most energetic bubble. This will remove any dependence on its origin (Type I or II).

2. Type I Mechanism

Only include bubbles created by pinch-off from conical cavity.

3. Type II Mechanism

Only include bubbles created by downward jet within the canopy of large drop splashes.

B. FUTURE EXPERIMENTS

1. More Data for this Experiment

In order to establish respectable statistics, more data needs to be taken. More data will also help to enforce the results of this work. The effect of a sloped surface for different raindrop sizes should be studied.

2. Multiple Raindrops

So far only single raindrops have been used for all experiments. Design a multiple drop experiment to determine if there is any interaction between the drops at impact (linear or nonlinear). The number and volume of the drops must be controllable in order to better understand the resulting spectra.

3. Multiple Hydrophones

Multiple hydrophones can be used to determine ranges of impacts or bubbles. This will determine the origin (bubble production mechanism) of all bubbles occurring later in time.

4. Capillary waves

Generate a roughened surface by creating capillary waves and then perform this same experiment. Compare the results of the smooth, sloped, and roughened (capillary) surface data.

5. Eliminate the % Correction Factor

Record the data series even if bubbles are not present. This will allow for a more accurate average total energy for a known number of drops and bubbles.

6. Extend the Listening Time

Use time delays of 320 ms or 640 ms to extend the time series to 640 ms or 960 ms, respectively. This will not affect the sampling rate.

APPENDIX A

The following three programs were written to analyze the single drop data collected in the NPS raindrop tank. The data was collected using ComputerScope© and stored in an ASCII file format. These files were stripped of extraneous headers and time information and stored as data files containing only the output voltage. (The time step is known and is input inside these programs). The stripped ASCII files are imported into MATLAB. These programs are written in the MATLAB processing language (MATLAB *.m files). All plotting routines can be easily changed within the program to present data any way the user desires.

The first program, **ANAL.M**, extracts:

the frequency of any bubble existing in the time series,

the time after impact of each bubble,

and the peak to peak voltage of each bubble in the time series.

The data is broken up into "dominant" and "all". It then saves the extracted data in matrices used in succeeding programs.

```
% Program ANAL.M
% Program to ANALyze data taken by ComputerScope and converted to ASCII.
% Calculates the frequency, time after impact, and Vpp of a particular bubble.
% Two mouse "ginputs" are required by the user. This is used for the freq.
% It also creates and saves (user chooses name of file) the data in a *.mat file
% for further manipulation in *.m files like delta.m.
clc
clear
clg
disp('In what directory will I find the data ')
direct = input('{i.e. full path [in single quotes]} ? ....');
disp(' ')
disp(' ')
start = input('Input number of starting file...');
stop = input('Input number of ending file...');
```

```
maxnum = stop - start + 1;
ftV=[ ];                    % empty matrix to allow the building of  the true data matrix
ftVdom=[ ];                 % empty matrix to allow the building of  the true data matrix
clc
disp('With what letter does the data file name start  ')
a=input('{i.e. r*.dat, s*.dat, etc} [in single quotes]...?');
for i = 1:maxnum;
    clg
    clc
    eval(['load ',direct,'\',a,int2str(start + i - 1), '.dat'])
    eval(['v = ',a,int2str(start + i - 1),';'])
    eval(['clear ',a,int2str(start + i - 1),';'])
    delt=20e-6;
    v = v - mean(v);
    plot(v)
    xlabel('n')
    ylabel('[volts]')
    title(['Drop # ',num2str(i),' for this data set.'])
    grid
    pause
    clc
    disp('Entering keyboard mode so that the user can determine the # of')
    disp('bubbles for this time series (in case of uncertainty).')
    disp(' ')
    disp('[CTRL-z] to exit keyboard mode')
    disp(' ')
    disp(' ')
    keyboard
    clc
    bub=input('How many bubbles in this series?...');

    for b=1:bub;
      clc
      low=input('Input lower data point (n) for plotting...');
      up=input('Input upper data point (n) for plotting...');
      subplot(211),plot(v)
      xlabel('n')
      ylabel('[volts]')
      title(['Drop # ',num2str(i),' for this data set'])
      grid
      subplot(212),plot(v(low:up))
      xlabel('n')
      ylabel('[volts]')
      title(['Bubble # ',num2str(bub),' for this drop'])
      grid
      pause
      disp(' ')
      check=input('Are these the correct limits?...1-Yes   2-No...');
      while check == 2
        clc
        disp(' ')
```

```
        disp('Last limits were... ')
        disp(' ')
        limits=[low up]
        disp(' ')
        low=input('Input lower data point for plotting...');
        up=input('Input upper data point for plotting...');
        clg
        subplot(211),plot(v)
        xlabel('n')
        ylabel('[volts]')
        title(['Drop # ',num2str(i),' for this data set'])
        grid
        subplot(212),plot(v(low:up))
        xlabel('n')
        ylabel('[volts]')
        title(['Bubble # ',num2str(bub),' for this drop'])
        grid
        pause
        clear check
        check=input('Are these the correct limits?...1-Yes   2-No...');
      end       % end while
      clc
          [mx,c]=max(v(low:up));
          mn=min(v(low:up));
          [xt yv]=ginput(2);
          freq=(abs(1/((xt(1)-xt(2))*delt)))/1000    % [kHz]
          t=((c+low)*delt)*1000                      % [ms]
          Vpp=abs(mx) + abs(mn)                      % [volts]
          disp(' ')
          ftVb=[freq t Vpp];   % freq, time, Vpp for each bubble
          disp(' ')
          if bub~=1;
            dom=input('Is this the dominant bubble of the series?...1-Yes   2-No...');
          else
            dom=1;
          end
          if dom==1;
            ftVdom=[ftVdom;ftVb];
          end
          ftV=[ftV;ftVb];
          clg
          plot(v)
          title(['Extra look at drop # ',num2str(i),' for this data set'])
          grid
          pause
          clc
    end          % next b
    clc
    clear v
end              % next i
mat=input('What name for the *.mat file [in single quotes] ? ....');
```

```
disp(' ')
disp('The matrix containing...freq [kHz]  t [ms]   Vpp [volts]...will be saved')
disp('for future uses (i.e. delta.m).  The variables will be ftV and ftVdom.')
disp(' ')
disp('Insert a disk into drive a: to receive the *.mat file...')
disp('[ENTER] to continue')
pause
!a:
eval(['save ',mat,' ftV ftVdom'])
!c:
clc
disp('It is now recommended to set up and run DELTA.M')
```

The second program, **DELTA.M,** uses the matrices formed in ANAL.M and calculates the theoretical damping constant (δ). Then the energy using δ and the 1/2 of Vpp (peak voltage) found in ANAL.M is calculated. Finally, many different combinations of data are plotted like Figures 4.1, 4.2 and 4.3.

```
% Program DELTA.M
% to be used after running ANAL.M and before ANAL2.M

% Creates monster matrix and calculates the damping constants and
% Energy based on these deltas   (Clay & Medwin text Ch 6)
% Plots different combinations of the data.

format short e
clc
clear
pack
clg
disp('Data consists of the matrices created in ANAL.M.  It is')
disp('the *.mat file containing the matrices consisting of:')
disp(' ')
disp('[ f (kHz)   t (ms)   Vpp (volts) ].')
disp(' ')
disp(' ')
disp(' What was the name of the *.mat file from')
file = input('ANAL.M {FULL PATH including filename (in single quotes)}.....?');
clc
disp('Where are the files d.dat and z.dat')
direct2 = input('{i.e. FULL PATH (in single quotes)}.....?');
eval(['load ',file]);
eval(['load ',direct2,'\','d.dat']);
eval(['load ',direct2,'\','z.dat']);

d=d./100;                              % [m]
z=z./100;                              % [m]

d=d(1:length(ftVdom(:,1)));            % [m]
z=z(1:length(ftVdom(:,1)));            % [m]

% rhoc = input('Input the Specific Acoustic Impedance (rhoc)...');
% diam = input('Input drop diameter [mm]...');
% gain = input('Input hydrophone gain...');
% ML = input('Input hydrophone Sensitivity  [V/Pa]...');
r0=1;          % 1 meter on axis
c = 1500;      % sound speed
rhoc = 1.54e06; % for seawater
ML = 2.66e-5;   % Hydrophone sensitivity (V/Pa) over 1-20 kHz
```

```
diam=4.6;
gain=100;

% calculate the damping constant based on a linear regression of the
% delta vs. freq (log-log plot) from Clay & Medwin

  del=.025 * ftVdom(:,1).^(1/3);       % ftVdom(:,1) is freq column [kHz]

% Calculate energy based on damping constant 'delta'

  r=sqrt(z.^2 + d.^2);                 % [m]
  k=2*pi*ftVdom(:,1)*1000/c;           % 1000 to convert to Hz
  CF=(r.^2)./(gain*ML*r0*z);
  NFC = (k.*r) ./ (sqrt((k.*r).^ 2 + 1));
  pax=NFC.*CF.*ftVdom(:,3)/2;          % 1 m on axis based on PEAK voltage
  E=((r.*pax).^2)./(1000*6*rhoc.*ftVdom(:,1).*del); % 1000 to convert to Hz

ftVdEdom=[ftVdom del E ];

% This part of delta.m plots different combinations of ftVdEdom.
% This matrix now consists of five columns:
% [f(kHz)  t(msec)  Vpp(Volts)  delta(damping constant)  Energy(joules)]
clc
disp('What type of surface was used for this data')
surf = input('{i.e. Smooth or Roughened (in single quotes)}.....?');
clc
name = input('What name do you want for the *.met file  {in single quotes}.....? ');
clc
disp('What name do you want for the *.mat file containing ')
name2 = input('the [ f t Vpp delta E ] matrix  {in single quotes}.....? ');
clc
m=mean(ftVdEdom);

% plot #1
% Dominant bubble Energy vs freq
%   l1=[0, 25, -12, -6];
%   axis(l1)
%   subplot(211),semilogy(ftVdEdom(:,1),ftVdEdom(:,5),'+')
%   tit=['Dominant Energy vs Frequency...',surf,' Sfc'];
%   title(tit)
%   xlabel('freq [kHz]')
%   ylabel('Energy [Joules]')
%   gtext(['Avg Energy = ',num2str(m(5)),' Joules'])

% plot #2
% Dominant bubble Energy vs time
%   l2=[0, 300, -12, -6];
%   axis(l2);
%   subplot(211),semilogy(ftVdEdom(:,2),ftVdEdom(:,5),'+')
%   subplot(212),semilogy(ftVdEdom(:,2),ftVdEdom(:,5),'+')
%   tit=['Dominant Energy vs Time after Impact...',surf,' Sfc'];
```

```
%   title(tit)
%   xlabel('time [msec]')
%   ylabel('Energy [Joules]')

% clc
% pause
% disp('Insert a disk into drive a to receive the *.met and *.mat files.')
% disp('ENTER to coninue')
% pause
% !a:
% eval(['meta ',name])     % plots #1 & #2
% !c:
% clg

% plot #3
% Dominant bubble Energy vs drop #

%   subplot(211),semilogy(ftVdEdom(:,5),'+')
%   tit=['Dominant Energy vs Drop number...',surf,' Sfc'];
%   title(tit)
%   xlabel('Drop #')
%   ylabel('Energy [Joules]')

% plot #4
% All bubbles...Freq vs time

   l4=[0, 300, 0, 25];                  % force the axis limits for direct comparisons
   axis(l4)
   subplot(211),plot(ftV(:,2),ftV(:,1),'+')
   gtext('ALL bubbles')
%   subplot(212),plot(ftV(:,2),ftV(:,1),'+')
   tit=['Frequency vs Time after Impact... ',surf,' Sfc'];
   title(tit)
   xlabel('t  [msec]')
   ylabel('freq [kHz]')

 pause
% !a:
 eval(['meta ',name])
 eval(['save ',name,' ftVdEdom'])
% !c:
 clc
 disp(' ')
 disp(' ')
 disp('It is now recommended that you set up and run ANAL2.M')
 disp(' ')
 disp('Thank you for playing DELTA.')
```

The final program, ANAL2.M, calculates and averages spectra for a series of drops and produces plots like those shown in Figures 4.4 and 4.5.

```
% Program ANAL2.M
% for rough and smooth surfaces

% program to ANALyze spectral level determination of raindrop data
% Converts bubble time series to power spectrum.  Outputs result.

clc
clear
clg
c = 1500;                % sound speed (use the correct sound speed for the salinity)
rhoc = 1.54e06;          % for seawater
ML = 2.66e-5;            % Hydrophone sensitivity (V/Pa) over 1-20 kHz
diam=4.6;
gain=100;
N=16384;
delt = 20 * 10^(-6);
disp(' ')
disp(' NOTE: Drop file names must be of the form r#.dat or s#.dat.')
disp('       The drop files must be numbered consecutively.')
disp(' ')
disp('       Ensure impact distances are in file d.dat. ')
disp('       and hydrophone depths are in file z.dat.')
disp('       D.DAT and Z.DAT MUST be in the same directory as your data files.')
disp('       Distances must be in a single column, in cm')
disp(' ')

dcheck = input('Did you update d.dat (distance) and z.dat (depth) files (1 = yes, 2 = no)..');
if dcheck ~= 1
  disp(' ')
  error('Update the files and rerun this program.')
end
clear dcheck;

clc

% diam = input('Input drop diameter (mm)...');
% gain = input('Input hydrophone gain...');
% ML = input('Input hydrophone Sensitivity  [V/Pa]...');
% N = input('Input number of points for FFT...');
% delt = input('Input sample period (time between samples, usec)...');
% delt = delt * 10^(-6);
pack
clc
```

```
surf = input('What type of surface?  (1-Smooth  2-Roughened)  ');
disp(' ')

if surf==2     % Rough Surfaces
  clc
  disp('DATA includes z.dat, d.dat. and r*.dat files')
  disp(' ')
  disp('In what directory will I find the DATA')
  direct = input('{i.e. full path [in single quotes]} ? ...');
  eval(['load ',direct ,'\d.dat;'])
  d=d./100;  % [m]
  eval(['load ',direct ,'\z.dat;'])
  z=z./100;  % [m]
  clc
  name = input('What do you want to call the meta file [in single quotes] ? ...');
  disp(' ')
  disp('What is the Sfc slope for this data (i.e. "5.5 degrees")')
  slope = input('[in single quotes] ?...');
  clc
  disp('For Roughened Surfaces...')
  start = input('Input number of starting file...');
  stop = input('Input number of ending file...');
  maxnum = stop - start + 1;
  perc = input('Input % of drops that produce at least one bubble...');
  perc = perc / 100;
  df = 1/(N * delt);
  Esum =zeros(1:(N/2));              % Initializing size of row vector
  f= (df.* [0:1:(N/2)-1])';
  k = (2 * pi .* f)./c;
  r0=1;                               % [m]

  for i = 1:maxnum;
    eval(['load ',direct,'\r',int2str(start + i - 1), '.dat'])
    eval(['v = ','r',int2str(start + i - 1),';'])
    eval(['clear ','r',int2str(start + i - 1),';'])
    v = v - mean(v);
    %  t=0:delt:(length(v)-1)*delt;
    V = abs(fft(v,N));
    clear v
    r(i) = sqrt(z(i)^ 2 + d(i).^ 2);                    % [m]
    NFC = (k.*r(i)) ./ (sqrt((k.*r(i)).^ 2 + 1));
    CF=((perc*r(i)^2)/(gain*ML*z(i)*r0));               % [Pa/v]
    Pax = CF .* NFC .* V(1:(N/2));                      % [Pa]  1 m on axis
    % Using eqn 41 from thesis by Ostwald
    Ef=((2*delt)./(N*df)).* Pax(1:N/2).^2;              % [Pa^2-s/Hz]
    clear Pax V
    E=((2*pi*r(i).^2)/(3*rhoc))*Ef;                     % [Joules/Hz]
    clear Ef
    Esum = Esum + E';                                   % for averaging purposes later
    clear E
  end
```

```
clear  CF NFC start stop N delt i surf r

  Eavg = Esum/maxnum;                                    % Average Energy density of all drops
  etot=sum(Eavg)*df;                                     % Evaluate the integral   eqn 42
  SL = (10*log10(Esum) + 120)';   % dB re 1 uPa^2/Hz
   clc
  disp('Four gtexts follow:  Sfc slope, Avg Energy, slope dependence, freq shift')
  disp('[Enter to continue]')
  pause
  ll=[0, 18, 0, 4e-13];
axis(ll)
%   subplot(211),plot(f./1000,Eavg);
%   subplot(212),plot(f./1000,Eavg);
  plot(f./1000,Eavg);
  xlabel('freq  (kHz)')
  ylabel('[Joules / Hz]')
  if maxnum==1;
    title(['Avg Energy Density for ',num2str(maxnum),' drop for Roughened Sfc'])
  else
    title(['Avg Energy Density for ',num2str(maxnum),' drops for Roughened Sfc'])
  end
  %(['Drop Diameter = ',num2str(diam),' mm'])
  gtext(['Sfc slope = ',slope])
  gtext(['Average Total Energy = ',num2str(etot),' [J]'])
  gtext('No significant dependence on slope')
  gtext('Spectrum shifts to higher frequencies')

%   subplot(212),plot(f(2:8190)./1000,SL(2:8190));
%   xlabel('freq  (kHz)')
%   ylabel('dB re 1 uPa^2 / Hz')
%   if maxnum==1;
%     title(['Spectrum Level for  ',num2str(maxnum),' drop'])
%   else
%     title(['Spectrum Level for  ',num2str(maxnum),' drops'])
%   end

  pause
%   clc
%   disp('Insert the *.met disk into A')
%   disp('[Enter to continue]')
%   pause
%   !a:
  eval(['meta ',name])
%   !c:
```

```
else      %  Smooth Surfaces

  clc
  disp('DATA includes d.dat, z.dat, and s*.dat files')
  direct = input('In what directory will I find the data {i.e. full path [in single quotes]} ? ....');
  eval(['load ',direct,'\d.dat'])
  eval(['load ',direct,'\z.dat'])
  d=d./100;   % [m]
  z=z./100;   % [m]
  name = input('What do you want to call the meta file [in single quotes]} ? ...');
  clc
  disp('For Smooth Surfaces...')
  start = input('Input number of starting file...');
  stop = input('Input number of ending file...');
  maxnum = stop - start + 1;
  perc = input('Input % of drops that produce at least one bubble...');
  perc = perc / 100;
  df = 1/(N * delt);
  Esum =zeros(1:(N/2));              % Initializing size of row vector
  f= (df.* [0:1:(N/2)-1])';
  k = (2 * pi .* f)./c;
  r = sqrt(z.^ 2 + d.^ 2);           % [m]
  r0=1;                               % [m]

  for i = 1:maxnum;
     eval(['load ',direct,'\s',int2str(start + i - 1), '.dat'])
     eval(['v = ','s',int2str(start + i - 1),';'])
     eval(['clear ','s',int2str(start + i - 1),';'])
     v = v - mean(v);
     %  t=0:delt:(length(v)-1)*delt;
     V = abs(fft(v,N));
     clear v
     i       % Progress Pointer for the user
     NFC = (k.*r(i)) ./ (sqrt((k.*r(i)).^ 2 + 1));
     CF=((perc*r(i)^2)/(gain*ML*z(i)*r0));      % [Pa/v]
     Pax = CF .* NFC .* V(1:(N/2));              % [Pa]  1 m on axis
     % Using eqn 41 from thesis by Ostwald
     Ef=((2*delt)./(N*df)).* Pax(1:N/2).^2;      % [Pa^2-s/Hz]
     clear Pax V
     E=((2*pi*r(i).^2)/(3*rhoc))*Ef;             % [Joules/Hz]
     clear Ef
     Esum = Esum + E';                           % for averaging purposes later
     clear E
  end

  clear  CF NFC start stop N delt i surf r

  Eavg = Esum/maxnum;                            % Average Energy density of all drops
  etot=sum(Eavg)*df;                             % Evaluate the integral   eqn 42
  SL = (10*log10(Esum) + 120)';                  % dB re 1 uPa^2/Hz
```

```
  disp(' ')
%  disp('Please insert the *.met disk into drive A [Enter to continue]')
%  pause
  clc
  disp('One gtext follows: Avg Energy')
  disp('[Enter to continue]')
  pause

l1=[0, 18, 0, 4e-13];
axis(l1)
%  subplot(211),plot(f./1000,Eavg);
  plot(f./1000,Eavg);
  xlabel('freq  (kHz)')
  ylabel('[Joules / Hz]')
  if maxnum==1;
    title(['Avg Energy Density for ',num2str(maxnum),' drop for Smooth Sfc'])
  else
    title(['Avg Energy Density for ',num2str(maxnum),' drops for Smooth Sfc'])
  end
  %gtext(['Drop Diameter= ',num2str(diam),' mm'])
  gtext(['Average Total Energy= ',num2str(etot),' [J]'])

%  subplot(212),plot(f(2:8190)./1000,SL(2:8190));
%  xlabel('freq  (kHz)')
%  ylabel('dB re 1 uPa^2 / Hz')
%  if maxnum==1;
%    title(['Spectrum Level for  ',num2str(maxnum),' drop'])
%  else
%    title(['Spectrum Level for  ',num2str(maxnum),' drops'])
%   end

  pause
%  !a:
  eval(['meta ',name;])
%  !c:
end
```

REFERENCES

Clay, C.S. and Medwin, H., *Acoustical Oceanography: Principles and Applications*, pp. 194-203, John Wiley and Sons Inc., [1977].

Franz, G.J.,"Splashes as Sources of Sounds in Liquids," *J. Acoust. Soc. Am.* **31**, pp. 1080-1096, [1959].

Jacobus, P.W., *Underwater Sound Radiation from Large Raindrops*, Master's Thesis, Naval Postgraduate School, Monterey, Ca, 93943, [1991].

Kurgan, A., *Underwater Sound Radiated by Impacts and Bubbles Created by Raindrops*, Master's Thesis, Naval Postgraduate School, Monterey, Ca, 93943, [1989].

Longuet-Higgins, M.S., "An Analytic Model of Sound Production by Raindrops," *J. Fluid Mechanics*, **214**, pp. 395-410, [1990].

Medwin, H., and Beakey, M.M., "Bubble Sources of the Knudsen Sea Noise Spectra," *J. Acoust. Soc. Am.*, **86**, pp. 1124-1130, [1989].

Medwin, H., Kurgan, A., and Nystuen, J.A., "Impact and Bubble Sound from Raindrops at Normal and Oblique Incidences," *J. Acoust. Soc. Am.*, **88(1)**, pp. 413-418, [1990].

Nystuen, J.A., McGlothin, C.C., and Cook, M.S., "The Underwater Sound Generated by Heavy Rainfall," Submitted to *J. Acoust. Soc. Am.*,[1992].

Nystuen, J.A., "An Explanation of the Sound Generated by Light Rain in the Presence of Wind," in *Natural Physical Sources of Underwater Sound* , ed., B.R. Kerman, Kluwar Academic Press, [to appear in 1993].

Oguz, H.N., and Prosperetti, A., "Bubble Entrainment by the Impact of Drops on Liquid Surfaces," *J. Fluid Mechanics*, **218**, pp. 143-162, [1990].

Ostwald, L.H., *Predicting the Underwater Sound of Moderate and Heavy Rainfall from Laboratory Measurements of Radiation from Single Large Raindrops*, Master's Thesis, Naval Postgraduate School, Monterey, Ca, 93943, [1992].

Pumphrey, H.C., Crum, L.A., and Bjorno, L., "Underwater Sound Produced by Individual Drop Impacts and Rainfall," *J. Acoust. Soc. Am.*, 85, pp. 1518-1526 [1989].

Scofield, C.D., *Oscillating Microbubbles Created by Water Drops Falling on Fresh and Salt Water: Amplitude, Damping, and the Effects of Temperature and Salinity*, Master's Thesis, Naval Postgraduate School, Monterey, Ca, 93943, [1992].

Snyder, D.E., *Characteristics of Sound Radiation from Large Raindrops*, Master's Thesis, Naval Postgraduate School, Monterey, Ca, 93943, [1990].

INITIAL DISTRIBUTION LIST

		No. Copies
1.	Defense Technical Information Center Cameron Station Alexandria, VA 22304-6145	2
2.	Library, Code 52 Naval Postgraduate School Monterey, CA 93943-5002	2
3.	Department of Physics Attn: Professor H. Medwin, Code PH/Md Naval Postgraduate School Monterey, CA 93943-5002	4
4.	Department of Oceanography Attn: Professor J.A. Nystuen, Code OC/Ny Naval Postgraduate School Monterey, CA 93943-5002	2
5.	Department of Physics Attn: Professor A.A. Atchley, Code PH/Ay Naval Postgraduate School Monterey, CA 93943-5002	1
6.	Dr. Ralph Baer Office of Naval Research (Code 1125 OA) 800 N. Quincy Street Arlington, VA 22217	1
7.	Mr. Harry Selsor Tactical Oceanography Warfare Support Office Bldg 1105, Rm 102 Naval Research Laboratory Code 311 Stennis Space Center, MS 39529-5004	1

8. Lt. Glenn Miller 1
c/o Mr. Nicholoas R. Miller
1803 Crosby Park Circle
Lawton, OK 73505

9. Lt. Peter Jacobus 1
c/o Dorothy Crain
116 Second St., Apt. 6
Pacific Grove, CA 93950

10. Lt. Clark Freise 1
Naval Research Laboratory
Code 7213
Washington, D.C. 20375-5320

DUDLEY KNOX LIBRARY
NAVAL POSTGRADUATE SCHOOL
MONTEREY CA 93943-5101

DUDLEY KNOX LIBRARY
3 2768 00308607 5